

Thermal Boundary Conditions for Heat Pipe Assisted Crystal Growth

by

Francis Johnson

B.S., Carnegie Mellon University (1996)

Submitted to the Department of Materials Science and Engineering
in partial fulfillment of the requirements for the degree of

Master of Science in Materials Science

at the

MASSACHUSETTS INSTITUTE OF TECHNOLOGY

February 1999

© Massachusetts Institute of Technology 1999. All rights reserved.

Author
Department of Materials Science and Engineering
January 15, 1999

Certified by
August F. Witt
Ford Professor of Engineering
MacVicar Faculty Fellow
Thesis Supervisor

Accepted by
Linn W. Hobbs
John. F. Elliot Professor of Materials
Chairman, Department Committee on Graduate Students

Science

Thermal Boundary Conditions for Heat Pipe Assisted Crystal Growth

by

Francis Johnson

Submitted to the Department of Materials Science and Engineering
on January 15, 1999, in partial fulfillment of the
requirements for the degree of
Master of Science in Materials Science

Abstract

Single crystal growth from the melt by conventional techniques such as the Czochralski and Bridgman methods requires the establishment of reproducible, controllable, and if possible, quantifiable boundary conditions. Such conditions are assumed to prevail in heat pipe based growth configurations. The purpose of this study was to assess the effectiveness of low temperature and high temperature heat pipes in approaching isothermality by comparative analysis with a stainless steel cylinder of identical geometry. The heat pipes and stainless steel cylinder were characterized with infrared thermography and contact thermocouples to assess their outer surface temperature and the radial thermal symmetry within the furnace cavity. The comparative analysis was carried out with surface coatings of identical emissivities to permit relative temperature measurements. A low-temperature (0 °C - 200 °C) heat pipe constructed of Cupronickel 70/30 with water as a working fluid, a high-temperature heat pipe (500 °C - 1100 °C) constructed of Inconel 601 with Na as a working fluid, and a 304 stainless steel blank were observed. Two datasets were collected: outer surface axial linescans of internally heated heat pipes and thermograms of a quartz charge located on the cavity of an externally heated heat pipe. The low temperature heat pipe exhibited axial and circumferential temperatures within 2 °C at setpoints between 100 °C and 200 °C. The high temperature heat pipe exhibited temperatures within 5 °C at a setpoint of 900 °C. The stainless steel cylinder exhibited an axial temperature difference of 20 °C at setpoints between 100 °C and 200 °C and a gradient of 100 °C at a setpoint of 900 °C. Both the high temperature heat pipe and the stainless steel cylinder caused a quartz charge to experience a radial profile between 28 to 40 °C depending on axial location. The stainless steel cylinder had a smaller gradient at the midpoint of the furnace cavity than the high temperature heat pipe.

Thesis Supervisor: August F. Witt
Title: Ford Professor of Engineering
MacVicar Faculty Fellow

Acknowledgments

I should like to thank my advisor, Prof. A.F. Witt, for his advice, guidance, and patience. To my colleagues Dr. P. Becla, Y. Zheng, Capt. T. L. Rittenhouse (USAF), N. A. Allsop (Oxon), and M. E. Wiegel for their friendship and encouragement. To my mother, Helen T., and my father, Francis P., for their understanding and love.

This work was partially supported by a NASA Graduate Student Researcher Fellowship administered by the Marshall Space Flight Center.

Ad Astra per Ardua.

Contents

| | | |
|----------|--|-----------|
| 1 | Introduction | 9 |
| 1.1 | Single Crystal Growth Technology | 9 |
| 1.1.1 | Single Crystals | 9 |
| 1.1.2 | Thermal Considerations for Crystal Growth | 10 |
| 1.1.3 | Czochralski Crystal Growth | 12 |
| 1.1.4 | Bridgman-Stockbarger Crystal Growth | 12 |
| 1.2 | Heat Pipes as Crystal Growth Furnace Components | 14 |
| 1.2.1 | Conventional Heat Pipes | 14 |
| 1.2.2 | Concentric Annular Heat Pipes | 18 |
| 1.2.3 | “Isothermal” Furnace Liners | 21 |
| 1.3 | Infrared Thermography | 24 |
| 2 | Procedure | 25 |
| 2.1 | Experimental Goals | 25 |
| 2.2 | Equipment | 25 |
| 2.2.1 | Dynatherm Isothermal Furnace Liners | 25 |
| 2.2.2 | Infrared Camera (Inframetrics 760 Scanner) | 26 |
| 2.2.3 | Digital Data Acquisition System (Azonix ScannerPlus) | 26 |
| 2.2.4 | Leeds and Northrup PID Controller | 27 |
| 2.3 | Setup | 27 |
| 2.3.1 | Outer Surface Temperature Measurements | 27 |
| 2.3.2 | Interior Radial Profile Measurements | 28 |
| 2.4 | Experimental Protocol | 30 |

| | | |
|----------|---|-----------|
| 2.4.1 | Emissivity Measurements of Surface Coatings | 30 |
| 2.4.2 | Control System Characterization | 31 |
| 2.4.3 | Outer Surface Temperature Measurements | 31 |
| 2.4.4 | Interior Radial Profile Measurements | 32 |
| 2.5 | Data Collection and Presentation | 33 |
| 2.5.1 | Data Collection | 33 |
| 2.5.2 | Presentation | 34 |
| 3 | Results | 35 |
| 3.1 | Outer Surface Temperature Measurements | 35 |
| 3.1.1 | Axial linescans recorded during ramp up to setpoint temperature | 35 |
| 3.1.2 | Axial linescans recorded around circumference of the heat pipe | 35 |
| 3.2 | Interior Radial Profiles | 42 |
| 3.2.1 | Infrared images of quartz charge within cavity | 42 |
| 4 | Discussion | 46 |
| 4.1 | Heat Pipe Performance | 46 |
| 4.1.1 | Outer Surface Measurements | 46 |
| 4.1.2 | Interior Radial Profiles | 47 |
| 4.2 | Infrared Thermography | 47 |
| 5 | Conclusions/Recommendations | 49 |

List of Figures

| | | |
|-----|--|----|
| 1-1 | Schematic of Czochralski Furnace (from Ueda, R., and Mullin, J.B., Crystal Growth and Characterization, North-Holland, Amsterdam, 1975, p.66) | 13 |
| 1-2 | Schematic of Bridgman-Stockbarger Furnace (from Brice, Crystal Growth Processes, Halsted Press, New York City, 1986) | 15 |
| 1-3 | Schematic of Conventional Heat Pipe (from Dunn and Reay, Heat Pipes, Pergamon Press, 1994, p. 3.) | 16 |
| 1-4 | Liquid Transport Factor vs Temperature for several working fluids (from Dunn and Reay, Heat Pipes, Pergamon Press, London, 1994, p. 29) | 17 |
| 1-5 | Heat Pipe Limitations vs. Temperature (from Chi, Heat Pipe Theory and Practice: A Sourcebook, McGraw-Hill, New York City, 1976, p. 8) | 18 |
| 1-6 | Schematic of Annular Heat Pipe (from Fahgri and Parvani, Journal of Thermophysics, Vol. 2, No. 3, pp. 165-171) | 19 |
| 1-7 | Reduced Pressure vs Axial Position (from Fahgri and Parvani, Journal of Thermophysics, Vol. 2, No. 3, pp. 165-171) | 21 |
| 1-8 | Axial Striations of Ga in Czochralski grown Ge grown without (a) and with (b) a heat pipe. Growth rate for (a) is 8.1 cm/hr with seed rotation at 6.14 rpm. Growth rate for b is 6.0 cm/hr with seed rotation at 17.1 rpm(from Martin, Witt, and Carruthers, J. of the Electrochemical Society, Vol. 126, No. 2, pp 284-287) | 23 |
| 2-1 | Setup for Outer Surface Temperature Measurements | 27 |

| | | |
|------|--|----|
| 2-2 | Setup for Interior Radial Profile Measurements | 29 |
| 3-1 | Axial linescans recorded at 1 minute intervals during ramp-up of High Temperature Heat Pipe to Setpoint 900 °C | 36 |
| 3-2 | Axial linescans recorded at 1 minute intervals during ramp-up of Stainless Steel Cylinder to Setpoint 900 °C | 36 |
| 3-3 | Axial linescans of Low Temperature Heat Pipe at Setpoint 100 °C | 37 |
| 3-4 | Axial linescans of Low Temperature Heat Pipe at Setpoint 200 °C | 37 |
| 3-5 | Axial linescans of Stainless Steel Cylinder at Setpoint 100 °C | 38 |
| 3-6 | Axial linescans Stainless Steel Cylinder at Setpoint 200 °C | 38 |
| 3-7 | Axial linescans of High Temperature Heat Pipe at Setpoint 900 °C | 39 |
| 3-8 | Axial linescans of Stainless Steel Cylinder at Setpoint 900 °C | 40 |
| 3-9 | Radial Profile of High Temperature Heat Pipe at (a)Top, (b)Midpoint, and (c) Bottom of Cavity | 43 |
| 3-10 | Radial Profile of Stainless Steel Cylinder at (a)Top, (b)Midpoint, and (c) Bottom of Cavity | 44 |

List of Tables

- 3.1 Contact Thermocouple Data (in °C) 40
- 3.2 Mean Surface Temperature as Measured by Infrared Camera (in °C) . 41
- 3.3 Standard Deviation of Surface Temperature As Measured by Infrared
Camera (in °C) 41
- 3.4 Power, in watts, required to maintain setpoint temperature 42

Chapter 1

Introduction

1.1 Single Crystal Growth Technology

1.1.1 Single Crystals

Single crystals are characterized by long-range periodic atomic order and absence of internal two-dimensional defects. In the abstract a single crystal can be visualized as a primitive lattice cell with infinite repetition along three orthogonal axes. Crystals with large dimensions along three orthogonal axes are called bulk crystals. In this thesis bulk crystals shall be referred to as single crystals.

Crystal defects are interruptions of long-range periodicity. Zero-dimensional defects, or point defects, are local interruptions in the atomic order such as vacancies, interstitial atoms, and substitutional atoms. Point defects are always present at thermodynamic equilibrium. One-dimensional defects, or dislocations, can be caused by stress applied to the crystal or condensation of point defects. Two-dimensional defects take the form of grain boundaries, twins, and surfaces; they generally demarcate regions of differing crystal orientation. Three-dimensional defects are voids and inclusions that usually signify the absence of a material or the presence of a another material.

Producing a crystal requires formation of a lattice structure by vapor/solid, melt/solid, or solution/solid phase transformation. It is also possible to grow single crystals by a

solid/solid transformations. This thesis is concerned with the growth of crystals from the melt, by solidification.

1.1.2 Thermal Considerations for Crystal Growth

The thermal boundary conditions present in crystal growth control the heat flow within the furnace. Heat transport directly or indirectly controls the density and distribution of impurities and defects within the solid crystal. Coupled with heat transport in the melt and furnace is mass transport due to convective flows and diffusion in the solid. The thermal boundary conditions in crystal growth furnaces can be expressed as axial and radial temperature profiles. Occasionally it is implicitly assumed that the temperature profile of the furnace is radially symmetric, but this is not normally the case.

Typically crystal growth furnaces are designed to primarily control the axial temperature profile. A control system is frequently configured to have its sensing element near the bottom of the crucible containing the charge. Power input to the heating element is adjusted to maintain the temperature of that element at a setpoint.

In contrast, the radial temperature gradient is not usually actively controlled. Its character is determined by furnace design and crucible placement. The radial temperature profile is coupled to the axial profile through heat transport in the melt. Sharp axial gradients lead to high rates of heat transport in the melt. Higher rates of transport near the wall result in a radial temperature gradient that differs in magnitude through the crystal.

Crystal growth from the melt will create a solid/liquid interface. The character of this interface determines many of the properties of the product crystal. Not only shape but also defect formation and composition are controlled by the interface which is controlled by heat transfer.

Interfacial stability is controlled by the degree of undercooling present in the liquid phase. A condition called constitutional supercooling leads to non-stable interfaces in multicomponent systems. High axial temperature gradients are used to avoid this effect and to achieve stable growth interfaces.

High axial temperature gradients can lead to supersaturation of point defects in the solid. If these defects are of the Schottky type they can condense to form clusters, dislocation loops, and mobile dislocations. Impurities can condense to form precipitates.

Carruthers[2] studied the origin of convective temperature oscillations in crystal growth melts. Crystal melts were examined as a function of the dimensionless Rayleigh number, N_{Ra} , which is defined as

$$N_{Ra} = N_{Pr}N_{Gr} \quad (1.1)$$

The Prandtl number, N_{Pr} , is defined as the ratio of kinematic viscosity, ν , and thermal diffusivity, κ :

$$N_{Pr} = \frac{\nu}{\kappa} \quad (1.2)$$

The Grashof number, N_{Gr} , is a measure of the horizontal (with respect to gravity) temperature gradient:

$$N_{Gr} = \frac{gK\Delta T_H\ell^3}{\nu^2} \quad (1.3)$$

where g is gravitational acceleration, K is thermal conductivity, ΔT_H is the horizontal temperature gradient, ℓ is a characteristic length, and ν is the kinematic viscosity.

Metal and semiconductor melts have low Prandtl numbers, on the order of 0.01, whereas molten oxides have Prandtl numbers on the order of 1. The thermal boundary conditions a melt experiences will determine the temperature gradients and are reflected in the Grashof number. This in turn can be used to compute the Rayleigh number for a melt. There exists for melt systems a critical Rayleigh number (N_{Ra}^C) that marks the transition from stable convective flows to rapidly oscillating or turbulent flows. Carruthers described several models that can be used to predict (N_{Ra}^C), the onset of turbulent convective flows.

Non-symmetric radial temperature gradients in the growing crystal can impair crystal quality. Thermal strains can be caused by thermoelastic stress fields, which lead to formation of dislocations which are detrimental to the performance of elec-

tronic devices. In severe cases of the thermal strain, the ultimate tensile strength of the material can be exceeded causing the crystal to crack. Jordan, Caruso and Von Neida[3] developed a quasi-steady state model for the axial and radial temperature profiles in liquid-encapsulated Czochralski grown GaAs crystals. These temperature profiles were used to predict thermoelastic stresses and the resulting dislocation density. Key to these results were the established thermal boundary conditions. A heat flux control system to control the radial heat input for Czochralski growth was developed by Kelley, Koai and Motakef[4]

1.1.3 Czochralski Crystal Growth

The most widely used crystal growth method is the Czochralski technique, also referred to as crystal-pulling. It is used, for example, to produce silicon and gallium arsenide for the manufacture of electronic devices. In this technique a crystal is grown by contacting a crystal seed onto the melt and pulling it upward through an axial temperature gradient. It is important to control the axial and radial temperature profiles in the solid crystal to minimize thermal strains. The temperature profiles in the liquid will control the convective transport of heat and mass to the interface. Radial homogeneity is expected to be enhanced by rotation of the crystal and/or crucible. This sets up a uniform heat and mass boundary layer in the liquid in front of the interface. Rotation in the presence of a radial thermal non-uniformity can cause striations. Figure 1-1 is a schematic of a Czochralski furnace that illustrates conductive, convective and radiative heat fluxes.

1.1.4 Bridgman-Stockbarger Crystal Growth

Bridgman-Stockbarger growth differs from Czochralski growth by solidifying the molten charge in a confining crucible through displacement in a thermal gradient. In general an axial gradient is maintained in a diabatic region. The interface is positioned in the region and either the charge or the gradient is displaced leading to solidification. In vertical Bridgman-Stockbarger growth the crucible (or ampoule) is translated along

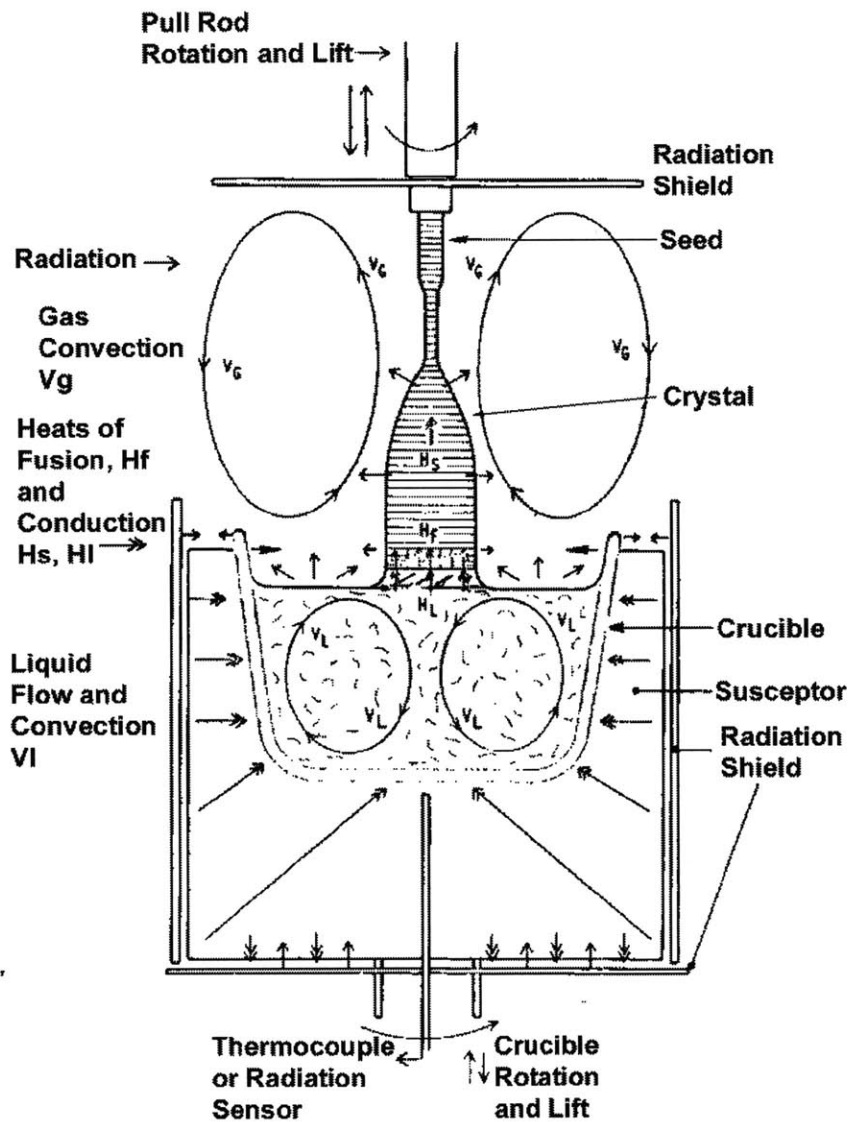


Figure 1-1: Schematic of Czochralski Furnace (from Ueda, R., and Mullin, J.B., Crystal Growth and Characterization, North-Holland, Amsterdam, 1975, p.66)

the axis of the furnace cavity while the temperature controllers maintain the thermal gradients at a constant value. The chances of achieving a single crystal are maximized by placing a seed crystal at the bottom of the crucible or ampoule. Figure 1-2 is a schematic of a vertical Bridgman-Stockbarger furnace. A variant of Bridgman-Stockbarger is the gradient freeze method in which the sample is held stationary while the setpoints in the heater zones are adjusted. This causes the interface to travel down the crystal crucible or ampoule. Gradient freeze furnaces are easier to construct than Bridgman-Stockbarger but have the disadvantage of a less well-controlled radial profile.

1.2 Heat Pipes as Crystal Growth Furnace Components

1.2.1 Conventional Heat Pipes

Heat pipes are high thermal conductivity devices of composite construction. A conventional heat pipe is an enclosed, evacuated cavity that contains a wick and a working fluid. A heat pipe can be divided into evaporator, adiabatic, and condenser zones. Heat is conducted through the wall of the evaporator into the wick and vaporizes the working fluid which acquires the latent heat of evaporation. Vapor flows through the adiabatic zone and condenses in the condenser zone. The latent heat of condensation is conducted through the wall of the condenser. The condensed working fluid is returned from the condenser to the evaporator through the wick. Fluid return is primarily driven by a difference in capillary pressure in the porous wick between the saturated condenser and the evaporator. Gravity can also drive fluid return. Figure 1-3 is a schematic of a conventional heat pipe.

Heat pipes were first theoretically described by G.M. Grover at Los Alamos National Laboratories in 1964[5]. They were originally developed for space nuclear power[6]. Today they are widely used for cooling of electronic packages[7]

A heat pipe operates when the capillary pressure gradient ΔP_c , exceeds the sum

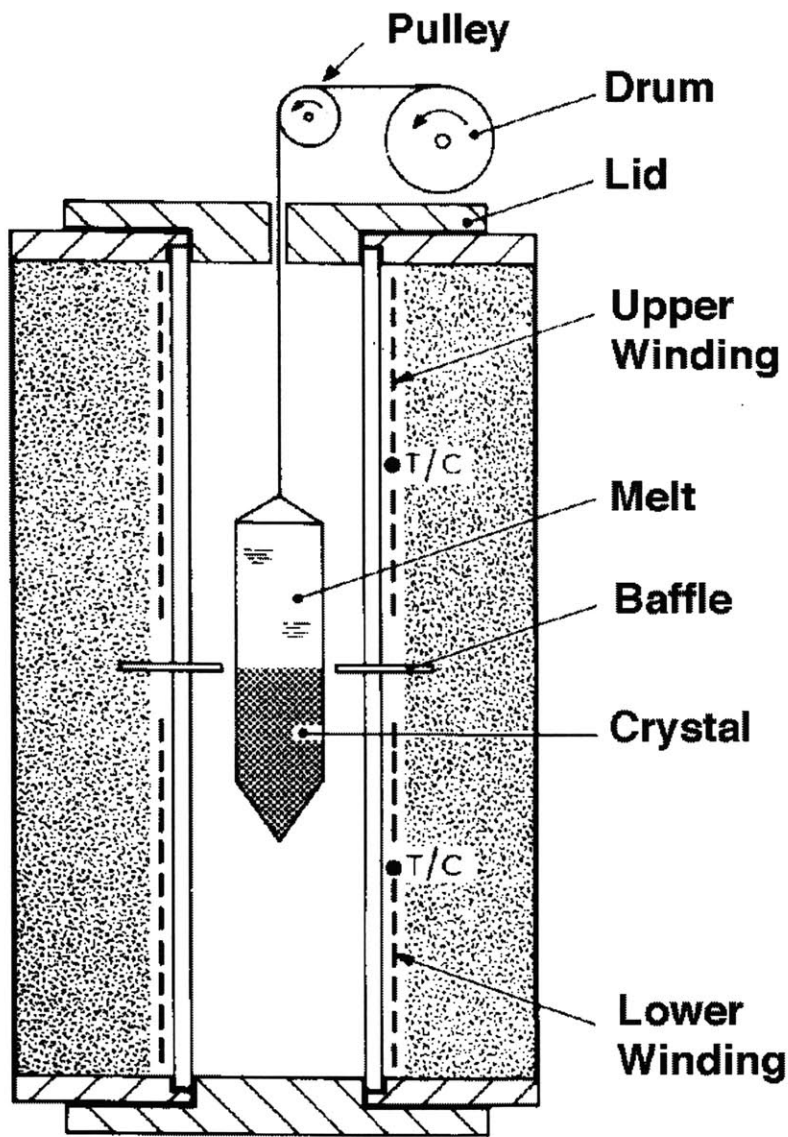


Figure 1-2: Schematic of Bridgman-Stockbarger Furnace (from Brice, Crystal Growth Processes, Halsted Press, New York City, 1986)

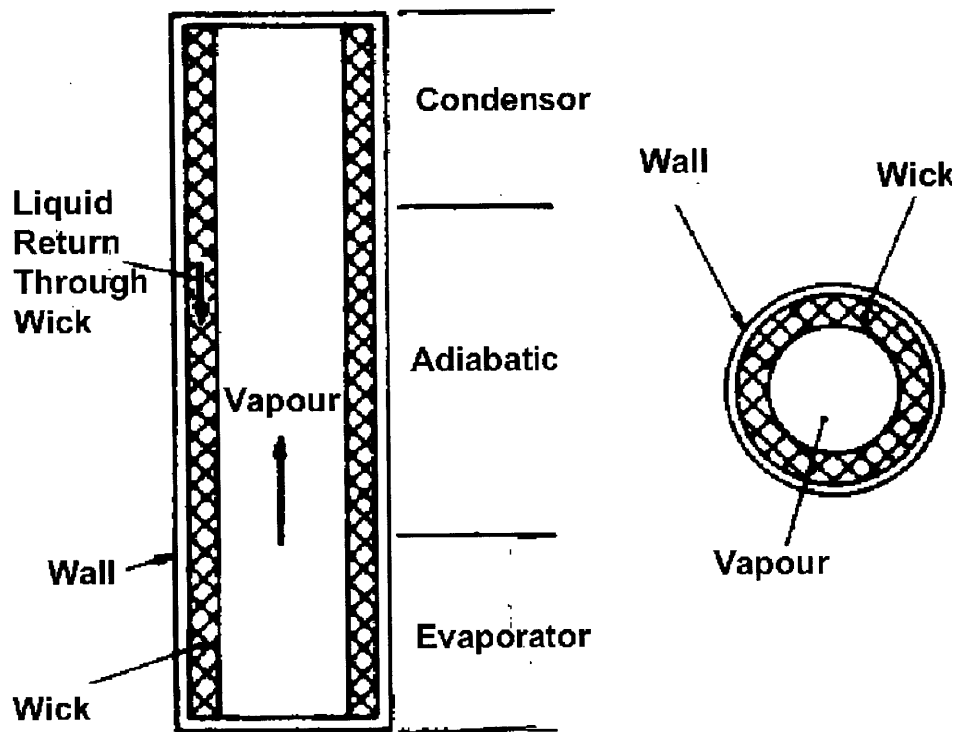


Figure 1-3: Schematic of Conventional Heat Pipe (from Dunn and Reay, Heat Pipes, Pergamon Press, 1994, p. 3.)

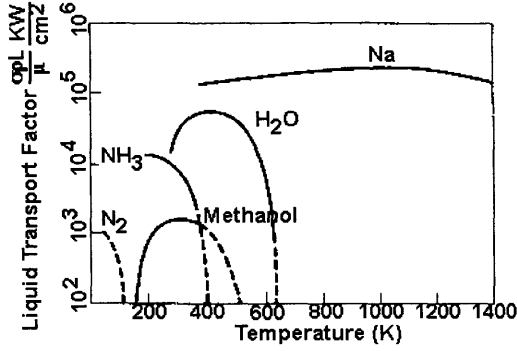


Figure 1-4: Liquid Transport Factor vs Temperature for several working fluids (from Dunn and Reay, Heat Pipes, Pergamon Press, London, 1994, p. 29)

of the pressure gradients in the liquid and vapor phases and any gravitational head that exists[8]:

$$\Delta P_c \geq \Delta P_{liquid} + \Delta P_{vapor} + \Delta P_{gravity} \quad (1.4)$$

It can maintain isothermal operation in regions where the vapor pressure gradient is small. The temperature gradient in the vapor is closely proportional to the pressure gradient. In a conventional heat pipe, the isothermal region is the adiabatic zone where the heat flux is small.

The capillary limitation to heat pipe operation occurs when the capillary pumping head is too small to return the working fluid from the condenser to the evaporator. The wick in the evaporator section dries out, interrupting the flow of vapor, and hence heat, to the condenser. This can cause a local hot spot in the evaporator that may damage the heat pipe. A figure of merit for heat pipes that depends only on the properties of the working fluid can be defined as:

$$\frac{\rho_\ell \sigma_\ell L}{\mu_\ell} \quad (1.5)$$

where ρ_ℓ is density of the working fluid, σ_ℓ is the surface tension of the working fluid, L is the latent heat of vaporization, and μ_ℓ is the viscosity of the working fluid. A fluid with a high figure of merit at a given temperature, such as Na at 900 °C, is preferable. Figure 1-4 is a plot of the figure of merit versus temperature for several working fluids.

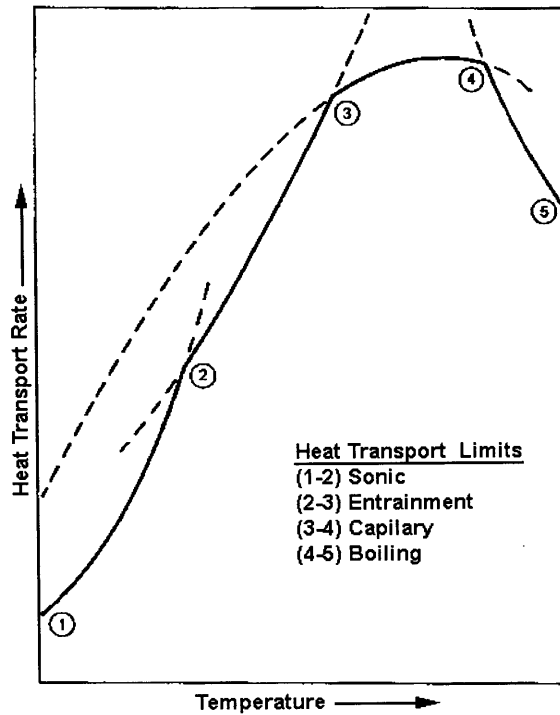


Figure 1-5: Heat Pipe Limitations vs. Temperature (from Chi, Heat Pipe Theory and Practice: A Sourcebook, McGraw-Hill, New York City, 1976, p. 8)

Other limitations to heat pipe operation include sonic, entrainment, and boiling limits. The temperature regions where these limitation become active are shown in Figure 1-5. The sonic limitation occurs when vapor exits the evaporator at a velocity greater than the local speed of sound. The entrainment limit occurs when the vapor flow exerts a shear force on the liquid/vapor interface which causes droplets of working fluid to become entrained in the vapor flow. The boiling limitation occurs when the working fluid begins to boil in the wick rather than evaporating from the surface.

1.2.2 Concentric Annular Heat Pipes

Conventional heat pipes have been widely discussed in the literature, with over three thousand journal articles and ten international conferences devoted to them. However, little attention has been paid to the class of heat pipes used in crystal growth: concentric annular heat pipes.

In crystal growth, a special geometry of heat pipe is used. The design concept is

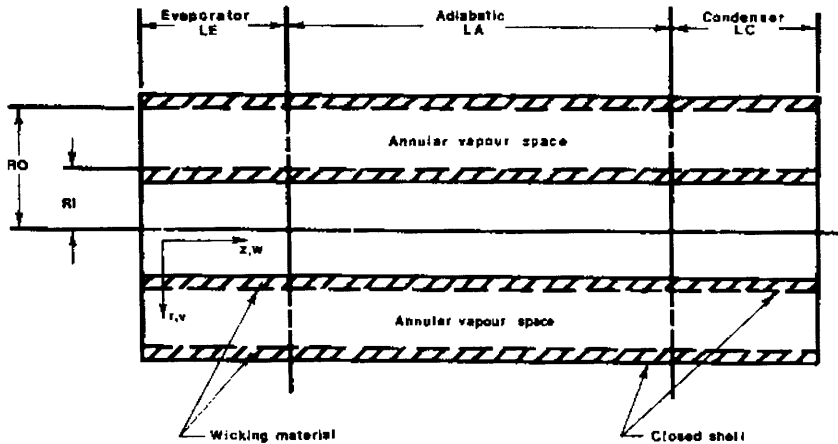


Figure 1-6: Schematic of Annular Heat Pipe (from Faghri and Parvani, Journal of Thermophysics, Vol. 2, No. 3, pp. 165-171)

to maintain an isothermal environment around the circumference of molten charge and a growing crystal while controlling the axial temperature profile.

Annular heat pipes are constructed from two coaxial cylinders of unequal diameter. The cylinders are joined at the ends by caps. The annulus between the cylinders is evacuated and filled with a wick and working fluid. Faghri[10] terms these heat pipes “concentric annular heat pipes.” Chi[9] mentions their operation in furnaces as placing heater elements on the outer wall of the heat pipe and a charge inside the inner cylinder. The latent heat of vaporization stored in the working fluid is available to be released upon condensation on the inner wall which minimizes the circumferential and axial temperature gradients (Figure 1-6).

Faghri[10, 11, 12, 13] has extensively investigated the operation of concentric annular heat pipes. Their potential for high heat flux to the inner wall surface is considered rather than their application to crystal growth.

The fluid dynamics of the working fluid in the vapor space was modeled using numerical techniques. A computer code with a finite difference algorithm was used[12].

The Navier Stokes equations in cylindrical coordinates are used to model momentum flow in the vapor phases with a parabolic equation of motion. Boundary conditions are selected that model evaporation or condensation as flow through porous walls into the evaporator or condenser.

Faghri solves these equations numerically for a variety of heat pipe geometries and inlet/outlet conditions, modeled by a radial Reynolds number defined at the outer and inner walls as:

$$Re_O = \frac{\rho R_O V_{OW}}{\mu} \quad (1.6)$$

$$Re_I = \frac{\rho R_I V_{IW}}{\mu} \quad (1.7)$$

The parabolic equations of motion predict for all conditions a pressure drop through the evaporator. Pressure drops through the condenser as well except at large Reynolds numbers and hence heat flows. In that case pressure recovery is predicted near the end of the condenser.

Faghri and Parvani[13], using a numerical solution of elliptical equations, extended this analysis by including the radial diffusion terms into the equation of motion. Power input and output is represented by fluid flows in to or out of the evaporator or condenser by a radial Reynolds number. The advantage is that all three sections of the heat pipe can be solved for simultaneously.

For small radial Reynolds numbers (< 10) the pressure profiles within the heat pipe decrease monotonically from the evaporator. The slope of the pressure drop is linear in the adiabatic zone with smaller, less constant slopes in the evaporator and condenser.

As the radial Reynolds number rises above 10, pressure recovery can occur within the condenser. At very high radial Reynolds numbers, corresponding to high heat fluxes, the pressure distribution changes dramatically. The pressure is seen to fall from the evaporator and rise in the condenser. What is most interesting for this thesis is the flat slope of pressure in the adiabatic zone. A flat temperature profile, coupled with vapor/liquid equilibrium, will lead to a flat temperature profile in the adiabatic zone. This provides for the nearly isothermal operation of concentric annular heat pipes. Figure 1-7 is a plot of reduced pressure vs. axial position that shows this condition.

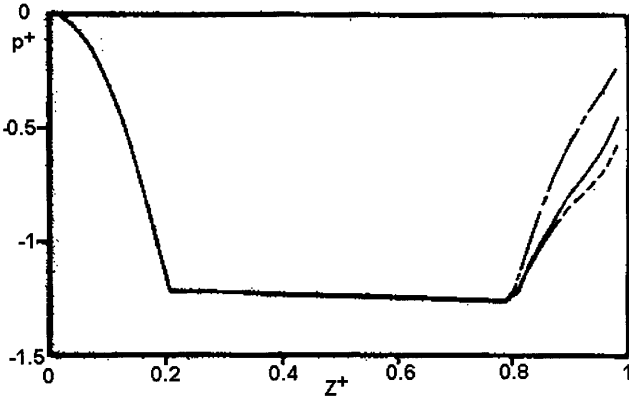


Figure 1-7: Reduced Pressure vs Axial Position (from Fahgri and Parvani, Journal of Thermophysics, Vol. 2, No. 3, pp. 165-171)

1.2.3 “Isothermal” Furnace Liners

Concentric annular heat pipes can be used as “isothermal” furnace liners. In this configuration a heat pipe is placed inside the cavity of a furnace. Heat is transmitted from the heating element of the furnace through the outer wall of the heat pipe. The working fluid evaporates from the wick on the outer wall and condenses on the inner wall. Heat is conducted through the inner wall and radiated into the central cavity of the heat pipe. There can also be conductive and/or radiative heat transport across the annulus between the inner and outer cylinders.

Bienert[14] describes a Na filled Inconel heat pipe operating with a power load of 1000 W at 883 °C. Under these conditions the Na vapor is near 1 atm pressure ($1.05 \times 10^5 Pa$). This leads to a viscous pressure loss of about 5.5 Pa. Bienert approximates the Clausius-Clapeyron equation as:

$$\frac{\Delta T}{T} = 0.1 \frac{\Delta P_v}{P} \quad (1.8)$$

Accordingly the temperature drop in the vapor phase is expected to be 0.006 °C.

For an isothermal furnace liner the wall thickness and thermal conductivity of the heat pipe must be used to predict the temperature profile in the pipe. This is

approximated by:

$$q = \left(\frac{k_w}{t_w}\right)\Delta T \quad (1.9)$$

where q is the heat flux, k_w is the thermal diffusivity through the wall, t_w is the wall thickness, and ΔT is the temperature difference along the heat pipe.

For the example calculation by Bienert the heat pipe had a length of 100 cm, an inner diameter of 2.0 cm, and an outer diameter of 2.6 cm. This yields a temperature difference of 6.4 °C for an Inconel heat pipe.

In practice the temperature profile is dependent on the thermal environment of the furnace. Heater element design and placement affect the heat flux and power throughput of the heat pipe as does placement of insulation. The geometry of the heat pipe can affect heat transport through radiative view factors and thermal conduction.

Bienert made calculations of the thermal profile of the previously mentioned heat pipe assuming radiative transport only. The axial temperature profile is symmetric with a maximum at the midpoint of the heat pipe. The axial temperature variation is less than 0.1 ° C within 12.5 cm of the midpoint and less 1.0 ° C within 22.5 cm of the midpoint.

Bienert conducted an experiment on a sodium heat pipe with an inner diameter of 7.8 cm and a length of 61 cm. A thermocouple probe was moved along the axis of the heat pipe, radiatively coupled to the walls. When heavily insulated with 10 cm of insulation material and 2 radiation shields the profile was isothermal within 0.025 ° C. Without insulation the measured temperature profile closely approached the calculated profile for a heat pipe without insulation.

Martin, Witt and Carruthers[15] applied a Na heat pipe to the Czochralski growth of Ga-doped Ge. The goal was to minimize radial dopant segregation effects by eliminating growth rate transients during rotational crystal pulling originating from radial thermal asymmetry in the molten charge. The investigators found that introducing a heat pipe into the hot zone of a Czochralski furnace was effective in reducing radial composition fluctuations by an order of magnitude. Figure 1.2.3 shows the reduction of Ga concentration fluctuations due to growth with a heat pipe. This allowed

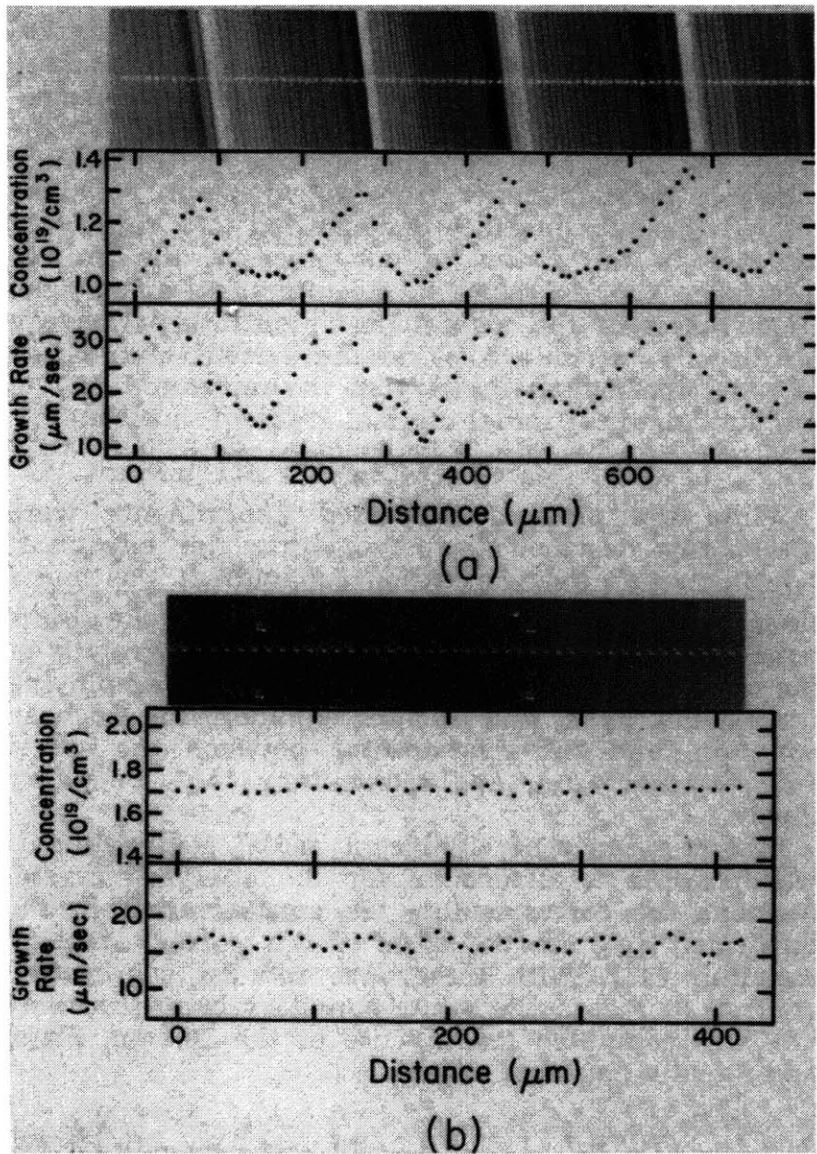


Figure 1-8: Axial Striations of Ga in Czochralski grown Ge grown without (a) and with (b) a heat pipe. Growth rate for (a) is 8.1 cm/hr with seed rotation at 6.14 rpm. Growth rate for b is 6.0 cm/hr with seed rotation at 17.1 rpm (from Martin, Witt, and Carruthers, J. of the Electrochemical Society, Vol. 126, No. 2, pp 284-287)

confirmation of the applicability of the Burton, Prim, and Slichter relation[16] for computing the solute boundary layer thickness from the steady-state growth rate.

Yemendijan and Lombos[17] constructed a heat pipe assisted zone melter for the growth of GaAs crystals. The zone melting technique[18] differs from other crystal growth techniques by the use of two solid/liquid interfaces that defines a liquid zone in the crystal surrounded by solid. A Na filled, stainless steel heat pipe was used to maintain an isothermal region (at 610 ° C) in an As reservoir connected to the growth ampoule. The As vapor pressure was therefore kept constant in the ampoule.

1.3 Infrared Thermography

Infrared thermography is based on the formation of images from infrared radiation collected by an optical system. Quantitative temperature information can be obtained when materials parameters, such as emissivity, are known. Infrared thermography is a non-contact measurement technique that does not disturb the thermal environment of the system being observed. The spatial resolution of the image is determined by the rastering capability of the scanning mechanism and the wavelength band of infrared radiation that is measured. The temporal resolution is limited by the scanning speed of the optical system and approaches real-time data acquisition. Temperature resolution is limited by the sensitivity of the infrared detector and the associated electronics.

Wargo and Witt[19] developed a thermal imaging technique to measure in-situ melt temperature during liquid-encapsulated-Czochralski growth of GaAs. A CCD camera with narrow bandpass filter set at 633 nm produced an image formed from the radiance of the melt. The system achieved a temperature resolution better than 0.5 ° C from 1000 to 1500 °C and a spatial resolution of better than 0.55 mm. The system was used to measure temperature stability of the GaAs melt as well as the radial temperature distribution in the crucible.

Chapter 2

Procedure

2.1 Experimental Goals

The experimental goals of this work were to measure the temperature profiles of concentric annular heat pipes acting as “isothermal” furnace liners. These results were compared with similar measurements of a stainless steel cylinder with identical dimensions to the heat pipes. Infrared thermography was employed to collect high spatial-resolution data in real time.

Outer surface temperature measurements were collected on heat pipes heated through the inner surface. Radial profiles were measured on a quartz charge placed in the heat pipe cavity.

2.2 Equipment

2.2.1 Dynatherm Isothermal Furnace Liners

The Dynatherm Corporation[20] markets concentric annular heat pipes under the name Isothermal Furnace Liners[21] (IFL’s). This work used two IFL’s. The first was a low temperature unit, model # 02-14-05. This unit was constructed of Cupronickel (70% Cu, 30% Ni) with water as the working fluid. It’s dimensions were 5.9 cm outer diameter, 3.5 cm inner diameter, and 12.4 cm in length. It’s temperature range was

100 °C to 250 °C. The second heat pipe was a high temperature unit, model # 11-14-05, constructed of Inconel 601 with Na as the working fluid. It's dimensions were identical to the low temperature unit; it's operating range was from 500 to 1100 °C. A 304 stainless steel cylinder was machined to identical dimensions to the heat pipes. The stainless steel cylinder was used to compare heat pipe action to bulk structural materials.

2.2.2 Infrared Camera (Inframetrics 760 Scanner)

Infrared temperature measurements were collected by a Model 760 Imaging Radiometer manufactured by Inframetrics Corporation[22]. The system used an electromechanically scanning HgCdTe infrared detector kept at 77 K. The detector was sensitive in the near infrared ($3 - 5 \mu m$) and the far infrared ($8 - 12 \mu m$) spectral bands. The temperature measurement range was -20 to 400 °C in normal mode and 20 to 1500 °C in extended mode. The minimum detectable temperature difference was 0.2 °C, the worst case accuracy is $\pm 2^\circ\text{C}$ or $\pm 2\%$ of the measured temperature. The scanner produced a raster image of 194 by 256 pixels at 8 bit (256 levels) resolution. Images could be recorded in adjustable temperature spans from 2 to 1000 °C. The scanner could be operated from a built-in console or remotely by a computer with an RS-232 serial line connection. The scan rate was 7866 Hz horizontal and 60 Hz vertical.

2.2.3 Digital Data Acquisition System (Azonix ScannerPlus)

An Azonix[23] ScannerPlus was used to collect temperature measurements from point-contact thermocouples. The ScannerPlus was a programmable, expandable measurement instrument with 62 analog inputs, 37 math channels, 80 digital inputs, and 80 digital outputs. For this work the ScannerPlus was equipped with 10 thermocouple inputs and 1 reference junction. Type K Chromega/Alumega thermocouples with measurement span from -18 to 1371 °C were used. The ScannerPlus could be operated from a built-in console or remotely by a computer with an RS-232 serial line connection.

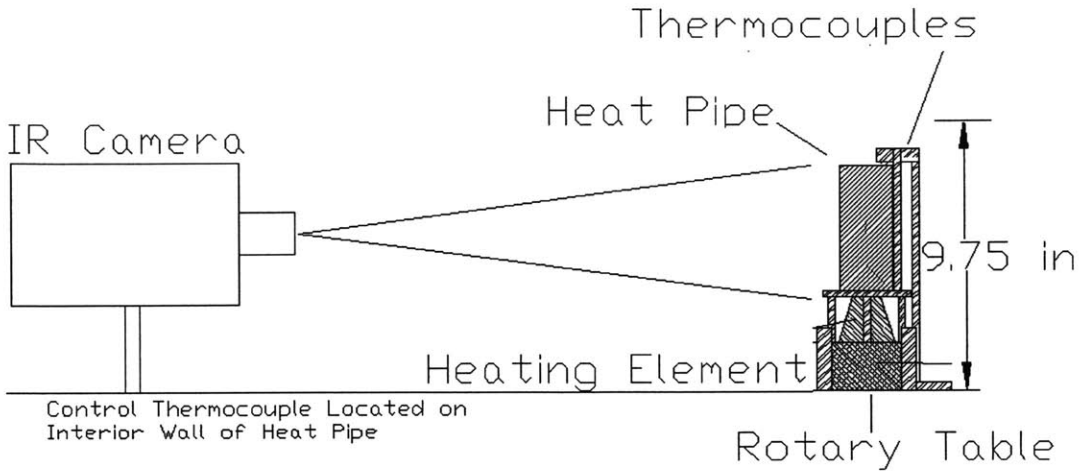


Figure 2-1: Setup for Outer Surface Temperature Measurements

2.2.4 Leeds and Northrup PID Controller

A Leeds & Northrup[24] Electromax V^{Plus} general purpose single-loop controller was used to control power input to the heating element to maintain a setpoint temperature. The Electromax V^{Plus} used a Proportional-Integral-Derivative (PID) control method whereby the control constants were found by Ziegler-Nichols tuning. The Electromax V^{Plus} was connected to a Halmar Electronics[25] Series LN-1 power supply configured to provide up to 30 amperes at 120 volts AC. Power output was controlled by a silicon-controlled-rectifier circuit that triggered in response to a control signal from the Electromax V^{Plus} .

2.3 Setup

2.3.1 Outer Surface Temperature Measurements

Figure 2-1 is a schematic of the setup used to collect outer surface temperature data. The concentric annular heat pipe was mounted on a rotary table to allow angular as well as axial temperature measurements. A heating element constructed of Kanthal wire was placed on the rotary table and extended into the heat pipe. The leads of the heating element were connected to the Halmar power supply. A type K control thermocouple was placed on the inner wall of the heat pipe at the midpoint of the

axis and is connected to the Electromax V^{Plus} controller. At this location the control thermocouple measured the heat pipe temperature with minimal end effects.

The heat pipe was supported above the rotary table by a stainless steel ring and was held in place by three set screws. The set screws minimized the contact area to the ring and minimized conductive heat transport. A stainless steel post supported a type K thermocouple at the midpoint of the axis of the heat pipe. The thermocouple was affixed to the post with double-bore alumina tube and supplied point-contact temperature information to the Azonix ScannerPlus.

For low temperature measurements the infrared camera directly imaged the heat pipe. For high temperature measurements radiative heat loss is reduced by surrounding the heat pipe with a Au-coated Pyrex tube that reflected infrared radiation back to the heat pipe. Au is a nearly perfect infrared reflector (reflectivity $\geq 99\%$). To make infrared measurements a Au-coated Pyrex plate was placed above the heat pipe to allow some radiation to be reflected to the IR camera. Some radiative heat was lost in this manner but that is unavoidable if full axial measurements were to be made.

2.3.2 Interior Radial Profile Measurements

Figure 2-2 is a schematic of the setup used to collect interior radial profile measurements. An existing furnace frame was modified to produce this setup. The aluminum frame contained a variable speed electric motor in its base and a worm gear in the spine. An assembly containing the heat pipe, Thermcraft[26] heating element, and Au-coated Pyrex tube was attached by a bracket to the worm gear. A charge was held stationary on the base of the frame parallel to the axis of the heat pipe assembly.

A Au-coated Pyrex plate is attached to the top of the frame at a 45 ° angle. This allowed the infrared camera to acquire an image of the charge looking down the axis of the heat pipe assembly. The infrared camera was placed on an adjustable mount adjacent to the furnace and is not shown in the Figure. Since the charge is held stationary, the camera only had to be focused on the charge once. Axial measurements could be made by moving the heat pipe assembly up and down with the worm gear.

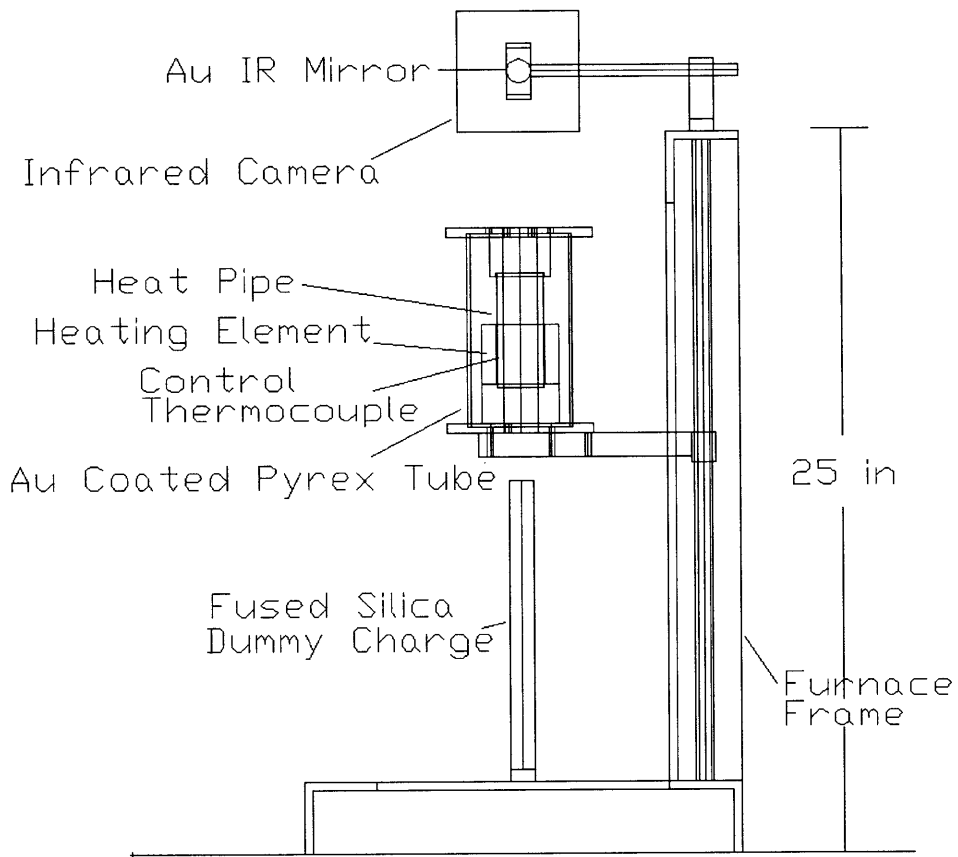


Figure 2-2: Setup for Interior Radial Profile Measurements

The Thermcraft heating element was comprised of two hemicylindrical shells whose power leads were connected in parallel to the Halmar controller. The shells were half the length of the heat pipe and covered the bottom half of the heat pipe, as per the recommendation of the heat pipe manufacturer. A type K control thermocouple was placed in between the outer surface of the heat pipe and the inner surface of the heating element, at the midpoint of the axial length of the heating element, which was $\frac{1}{4}$ of the axial length of the heat pipe. This placement was chosen as the point of maximum heat input to the heat pipe. The control thermocouple was connected to the Electromax V^{Plus} as well as the Azonix ScannerPlus to allow the heater temperature to be recorded.

2.4 Experimental Protocol

2.4.1 Emissivity Measurements of Surface Coatings

The infrared camera has the capability to correct for greybody emissivity through a software setting. Greybody emissivity is non-unity emissivity (non blackbody emissivity) that does not vary with angle or wavelength. The Inframetrics 760 manual described a technique for measuring greybody emissivity. Two power resistors, one 5Ω the other 10Ω were connected in parallel to a DC power supply. The resistors, heat pipe, and infrared camera were arranged so that the heated resistors and their reflections off the heat pipe were imaged. The camera was programmed to record the emission level for the source resistors and their reflections. The ratio of the differences of the levels is the reflectivity. Since, absent transmission, the reflectivity and emissivity must equal unity, the emissivity is calculated by:

$$e = 1 - \frac{10\Omega_{reflection} - 5\Omega_{reflection}}{10\Omega_{source} - 5\Omega_{source}} \quad (2.1)$$

2.4.2 Control System Characterization

The Electromax V^{Plus} controller is a PID controller that requires the control constants to be determined before operation. The operators manual describes how to do this. The power output of the controller is set at 100% and the control thermocouple is recorded every minute. The proportional band is $\frac{1}{3}$ the range of temperature achievable by the heater. The integral constant is the of the slope of the linear portion of the time-temperature curve, in minutes. The derivative control constant is the response lag, in minutes, caused by thermal capacitance of the heating element and heat pipe. These constants, in particular the integral constant, would have to be manually adjusted to ensure good control action.

The control thermocouple input on the Electromax V^{Plus} was calibrated with a nanovoltage source capable of three significant figures. The reference junction was located inside the housing on the circuit board and was measured with the Azonix ScannerPlus to remain at a constant 25 °C.

2.4.3 Outer Surface Temperature Measurements

Two sets of experiments were conducted to measure the outer surface temperature profiles. In the first set, a the low temperature heat pipe was compared against the stainless steel cylinder. In the second set, the high temperature heat pipe was compared against the stainless steel cylinder.

In both sets data was collected by the Azonix ScannerPlus and the infrared camera. The Azonix ScannerPlus measured the control thermocouple and a point contact thermocouple located at the midpoint of the axial length of the heat pipe on the outer surface. The infrared camera was operated in linescan mode with the measured line along the axial length of the heat pipe.

For the low temperature series both the heat pipe and the stainless steel cylinder were dip-coated with two coats of SpecPro 631-190 flat black paint. The emissivity of this coating was measured as 0.88 and this value was entered into the infrared camera.

Measurements were made for a series of set point measurements, 100, 125, 150, 175 and 200 °C. Temperature data was recorded from the Azonix ScannerPlus and infrared camera during ramp-up, at setpoint, and cool-down. During ramp-up and cool-down point-contact and linescan measurements were collected at 1 minute intervals. While the controller held the setpoint, circumferential point-contact and linescan measurements were made by rotating the heat pipe and heater at 10 °increments while keeping the infrared camera stationary.

For the high temperature series the heat pipe and stainless steel cylinder (with the flat black coating removed) were coated with Union Carbide Advanced Ceramics High-Purity Boron Nitride spray. This spray consisted of boron nitride powder with a binder that adhered to the surface of the heat pipe during ramp-up. The spray was found to perform adequately as a uniform thermal emitter. The emissivity measurement technique described above was not able to determine emissivity at high temperature because a high temperature reference source was not available. The infrared camera was set to an emissivity of unity.

The high temperature measurements were carried out at a setpoint temperature of 900 °C. The test assembly was surrounded by a Au coated Pyrex tube to minimize radiative heat loss. This obstructed the view of the infrared camera. A Au coated Pyrex mirror was placed at the top of the heat pipe where an inclined view of the heat pipe was available. Infrared linescans were measured from the reflected image in the mirror. The angle of reflection was not greater than 60 ° so the greybody assumption held. Linescan and point contact measurements were made during ramp-up, at setpoint, and during cool-down for the high temperature heat pipe and the stainless steel cylinder. Because of the high temperatures the rotary table could not be operated so circumferential measurements were not made.

2.4.4 Interior Radial Profile Measurements

To collect radial charge profiles a representative charge had to be found that would mimic the thermal characteristics of a real crystal charge yet provide controlled conditions for measurement. The charge material was chosen to be high-purity silica glass

(quartz). The material choice was made because quartz is transparent to infrared radiation up to $5\ \mu\text{m}$. This infrared transmittance is representative of oxides such as $\text{Bi}_{12}\text{SiO}_{20}$. The charge was 19 mm in diameter. The ratio of the inner diameter of the heat pipe and the diameter of the charge is typical of that used in Czochralski growth of single crystals.

Imaging the temperature profile of the quartz charge required separating the radiance of the interior of the dummy charge from that of the cross section being measured. To accomplish this an opaque coating of boron nitride was applied to the top surface of the charge. This allowed radial infrared emittance of the cross-section to be measured. A boron nitride layer also simulated the presence of a solid/liquid interface within the charge.

To setup the furnace the charge was radially centered in the heat pipe with calipers within 3 mm of the centerpoint. The heat pipe assembly was moved axially to place the boron nitride layer level with the top surface of the heat pipe. The setpoint temperature was set at $900\ \text{°C}$.

Measurements were made on both the high temperature heat pipe and the stainless steel cylinder. Measurements were made during ramp-up to the setpoint at 1 minute intervals and at ten axial positions along the length of the heat pipe while holding the setpoint. The infrared camera was used to collect images of the boron nitride layer as well as linescans of the diameter. The Azonix ScannerPlus was used to record the setpoint temperature during ramp-up.

2.5 Data Collection and Presentation

2.5.1 Data Collection

An IBM PC was used to command the Azonix ScannerPlus and infrared camera to download temperature information in real time over an RS-232 serial link. QBasic code was written to collect and store the temperature information for later analysis as a function of time and angular position

2.5.2 Presentation

Data was reduced from the raw data files using the MATLAB software package. Level information from the infrared camera was converted to temperature information. Plots of temperature vs. time and temperature vs. angular position were created from the Azonix Scanner plus data. Matrices of temperature vs axial and angular position were produced from the infrared data. These matrices could be displayed as maps or multi-line plots.

Chapter 3

Results

3.1 Outer Surface Temperature Measurements

3.1.1 Axial linescans recorded during ramp up to setpoint temperature

Figures 3-1 and 3-2 are axial linescans of the high temperature heat pipe and the stainless steel cylinder recorded while the controller ramped the setpoint temperature up to 900 °C. These linescans were recorded from the infrared camera along the length of the outer surface of the heat pipe. The stainless steel cylinder is seen to exhibit an axial gradient at all times during the ramp-up. In contrast, the slope of the high temperature heat pipe is seen to continuously flatten as the equilibrium temperature is approached.

3.1.2 Axial linescans recorded around circumference of the heat pipe

Figures 3-3, 3-4, 3-5, and 3-5 are axial linescans around the circumference of the low temperature heat pipe and stainless steel cylinders for setpoints of 100 °C and 200 °C. The plots contain 36 linescans recorded at 10 ° intervals around the outer circumferences of the cylinders. The plots show that the low temperature heat pipe

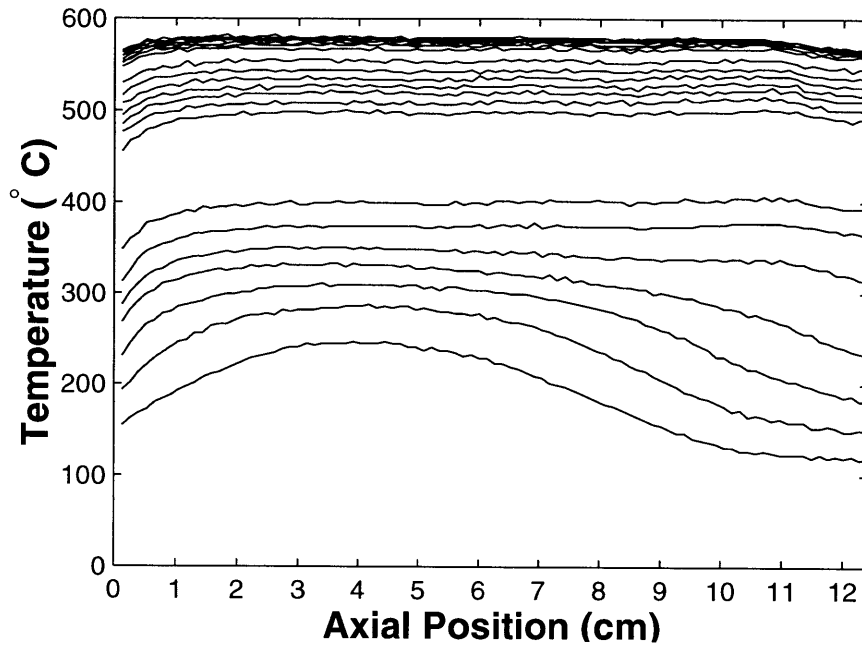


Figure 3-1: Axial linescans recorded at 1 minute intervals during ramp-up of High Temperature Heat Pipe to Setpoint 900 °C

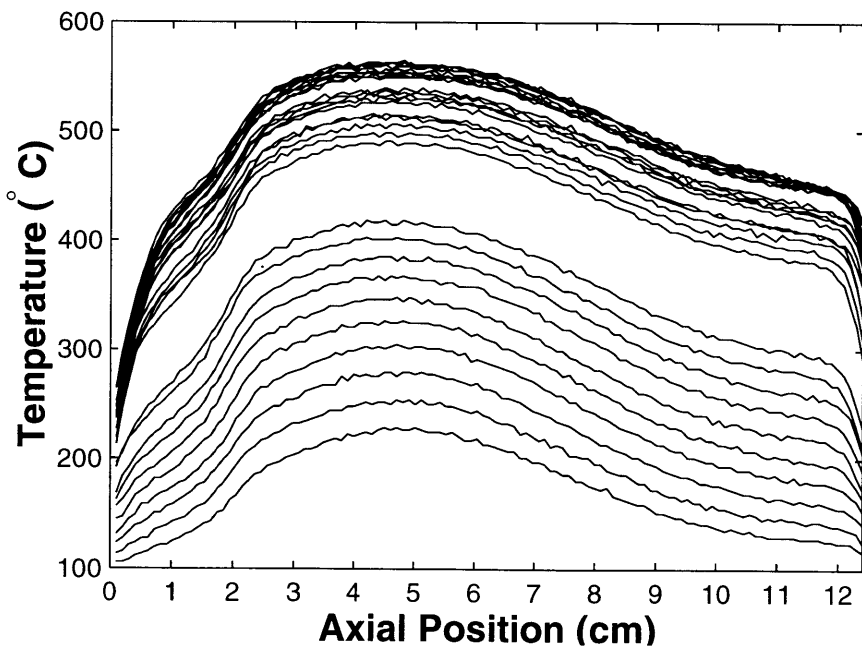


Figure 3-2: Axial linescans recorded at 1 minute intervals during ramp-up of Stainless Steel Cylinder to Setpoint 900 °C

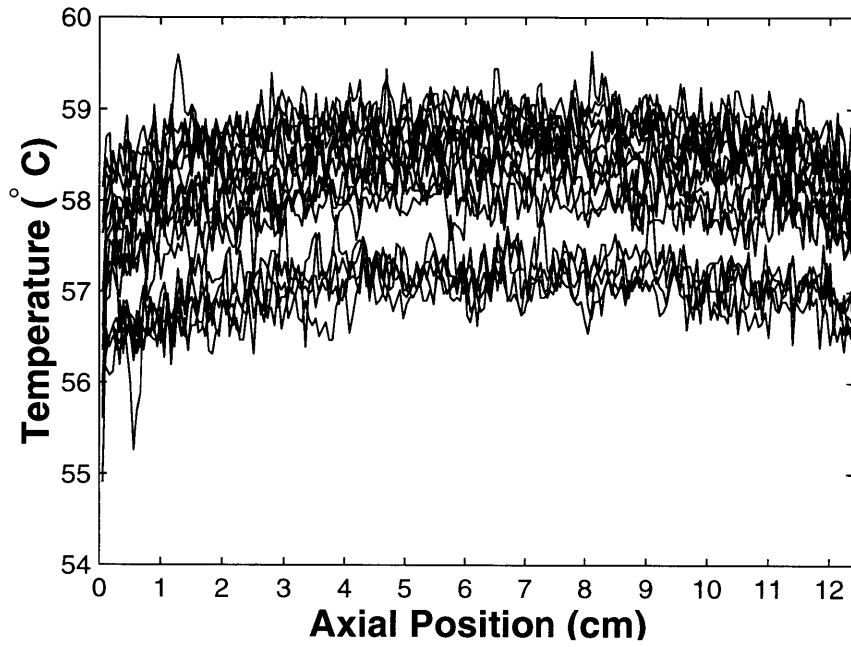


Figure 3-3: Axial linescans of Low Temperature Heat Pipe at Setpoint 100 °C

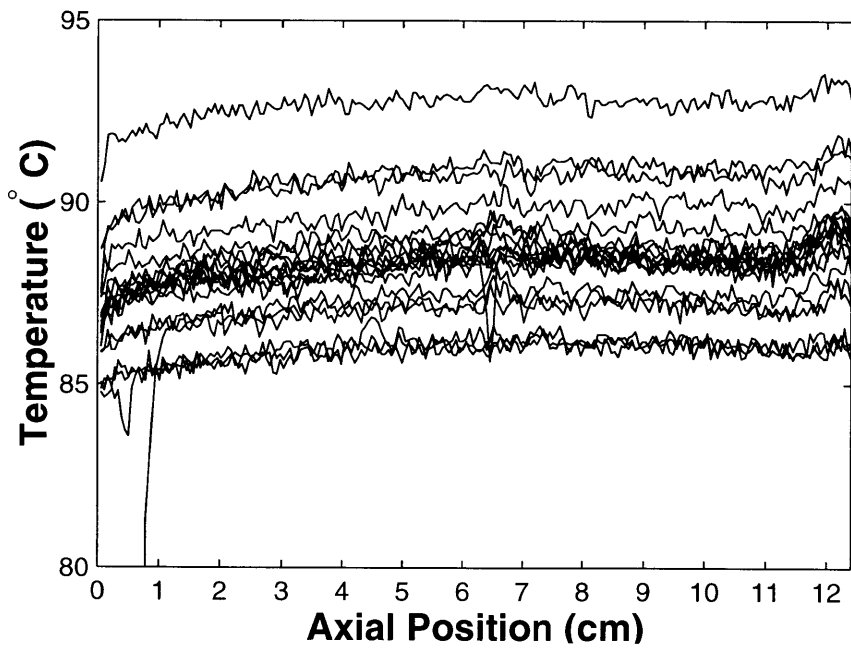


Figure 3-4: Axial linescans of Low Temperature Heat Pipe at Setpoint 200 °C

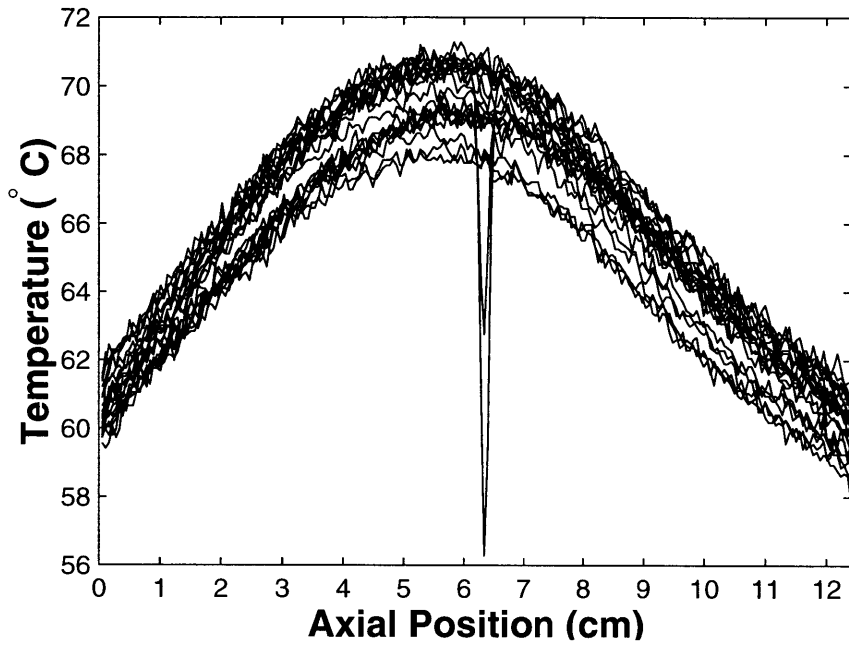


Figure 3-5: Axial linescans of Stainless Steel Cylinder at Setpoint 100 °C

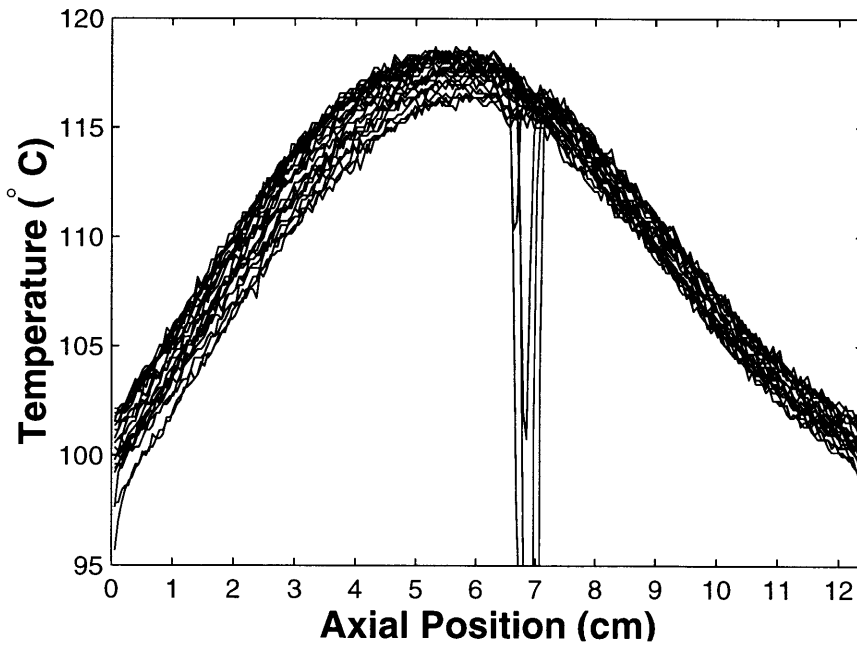


Figure 3-6: Axial linescans of Stainless Steel Cylinder at Setpoint 200 °C

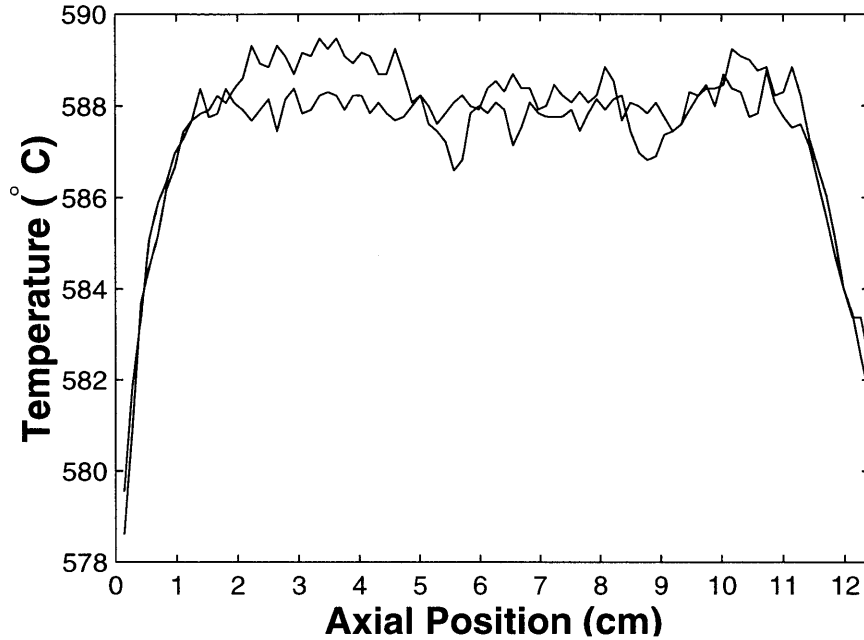


Figure 3-7: Axial linescans of High Temperature Heat Pipe at Setpoint 900 °C

more nearly approaches axial isothermality than the stainless steel cylinder. The low temperature heat pipe has a temperature variation of less than 0.5 °C while the stainless steel cylinder had a variation of 12 °C at 100 °C setpoint and 20 °C at the 200 °C setpoint. The outlier in the center of the stainless steel plots was due to a scratch in the surface coating caused by the contact thermocouple. The temperature also varied around the circumference. This variation was observed to be narrower for the stainless steel cylinder at 200 °C than for the other conditions.

Figures 3-7 and 3-8 are axial linescans of the high temperature heat pipe and stainless steel cylinder at a setpoint of 900 °C. Circumferential measurements were not made. The high temperature heat pipe shows an axial temperature variation of 5 °C near the ends of the heat pipe and less than 2 °C over 90% of the length. In contrast the stainless steel cylinder showed an axial temperature variation of 100 °C.

Table 3.1 shows the temperatures measured on the outer surface of the cylinders at the axial midpoint by a contact thermocouple. The setpoint thermocouple was located on the inner surface at the axial midpoint. In all cases there was a temperature gradient from the inner to outer surfaces. The relative magnitude of this gradient was

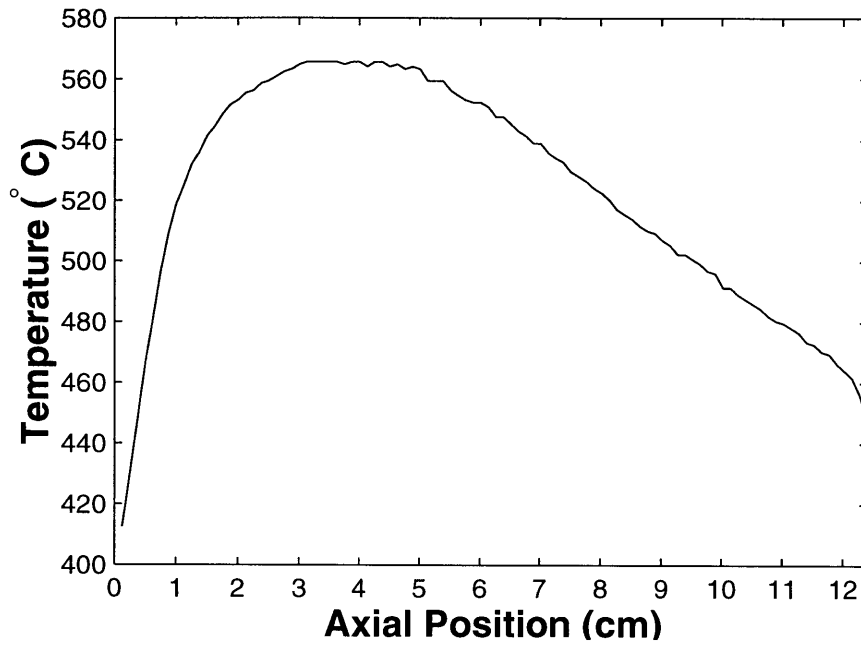


Figure 3-8: Axial linescans of Stainless Steel Cylinder at Setpoint 900 °C

| Setpoint | Low Temperature Heat Pipe | Stainless Steel Cylinder | High Temperature Heat Pipe |
|----------|---------------------------|--------------------------|----------------------------|
| 100°C | 43.1°C | 49.6°C | |
| 125°C | 49.4°C | 58.8°C | |
| 150°C | 58.8°C | 69.7°C | |
| 175°C | 55.0°C | 86.2°C | |
| 200°C | 63.3°C | 83°C | |
| 900°C | | 599.9°C | 658.7°C |

Table 3.1: Contact Thermocouple Data (in °C)

| Setpoint | Low Temperature Heat Pipe | Stainless Steel Cylinder | High Temperature Heat Pipe |
|----------|------------------------------|-----------------------------|-------------------------------|
| 100°C | 58.1°C | 65.6°C | |
| 125°C | 70.3°C | 81.1°C | |
| 150°C | 88.3°C | 99.6°C | |
| 175°C | 72.8°C | 112.6°C | |
| 200°C | 88.1°C | 110.0°C | |
| 900°C | | 521.0°C | 587.0°C |

Table 3.2: Mean Surface Temperature as Measured by Infrared Camera (in °C)

| Setpoint | Low Temperature Heat Pipe | Stainless Steel Cylinder | High Temperature Heat Pipe |
|----------|------------------------------|-----------------------------|-------------------------------|
| 100°C | 0.69°C | 3.29°C | |
| 125°C | 0.61°C | 4.18°C | |
| 150°C | 0.75°C | 5.05°C | |
| 175°C | 1.04°C | 6.35°C | |
| 200°C | 1.69°C | 5.80°C | |
| 900°C | | 39.8°C | 2.9°C |

Table 3.3: Standard Deviation of Surface Temperature As Measured by Infrared Camera (in °C)

larger for the low temperature heat pipe compared to the stainless steel cylinder, but smaller for the high temperature heat pipe compared to the stainless steel cylinder.

Table 3.2 shows the mean surface temperatures calculated from the linescans collected by the infrared camera. These values are an arithmetic average of the temperature data over the entire surface. Again, there are large gradients from the inner to outer surface. However, the temperatures recorded by the infrared camera differ from those of the contact thermocouple displayed in Table 3.1. For the low temperature sequence the infrared temperatures are higher than the thermocouple measurements, while for the high temperature sequence the infrared temperatures were lower. For the low temperature sequence this is most likely due to a sharp temperature gradient present in the thermocouple. The thermocouple in the high temperature sequence was surrounded by the Au-coated Pyrex tube insulator so this difference could be explained by the non-unity emissivity of the boron nitride coating.

Table 3.3 shows the standard deviation of the the surface temperature calculated from the linescans collected by the infrared camera. The standard deviation is used as

| Setpoint | Low Temperature Heat Pipe | Stainless Steel Cylinder | High Temperature Heat Pipe |
|----------|---------------------------|--------------------------|----------------------------|
| 100°C | 3.8 W | 6.7 W | |
| 125°C | 5.8 W | 9.9 W | |
| 150°C | 8.3 W | 13.5W | |
| 175°C | 11.5 W | 17.8W | |
| 200°C | 14.8 W | 23.5W | |
| 900°C | | | 1012 W |

Table 3.4: Power, in watts, required to maintain setpoint temperature

a statistical measure of the temperature variation of the heat pipe. The stainless steel cylinder is seen to exhibit a variability one order of magnitude greater than the heat pipes. The high temperature heat pipe is seen to have a larger standard deviation than the low temperature heat pipe. This may be caused by the lower temperature resolution of the infrared camera operating in the near infrared.

Table 3.4 compares the electrical power, in watts, required to maintain the heat pipes at the setpoint temperature. At low temperatures the stainless steel cylinder was observed to require more power than the low temperature heat pipe. At high temperatures on the order of a kilowatt of power was required to maintain the high temperature heat pipe at setpoint.

3.2 Interior Radial Profiles

3.2.1 Infrared images of quartz charge within cavity

Figure 3-9 displays infrared images collected at the top, midpoint and bottom of the cavity of the high temperature heat pipe. Figure 3-10 displays infrared images collected at the top, bottom and midpoint of cavity of the stainless steel cylinder. These figures are grayscale maps produced by MATLAB of the image data collected by the infrared camera. Black is the lowest temperature and white is the highest temperature. The temperature range was 50 °C with 256 grey levels or a resolution of 0.2 °per level. Contour lines were placed at 10 °C intervals. The radial gradients are smallest at the midpoint of the cavity. The shift in location of the maximum

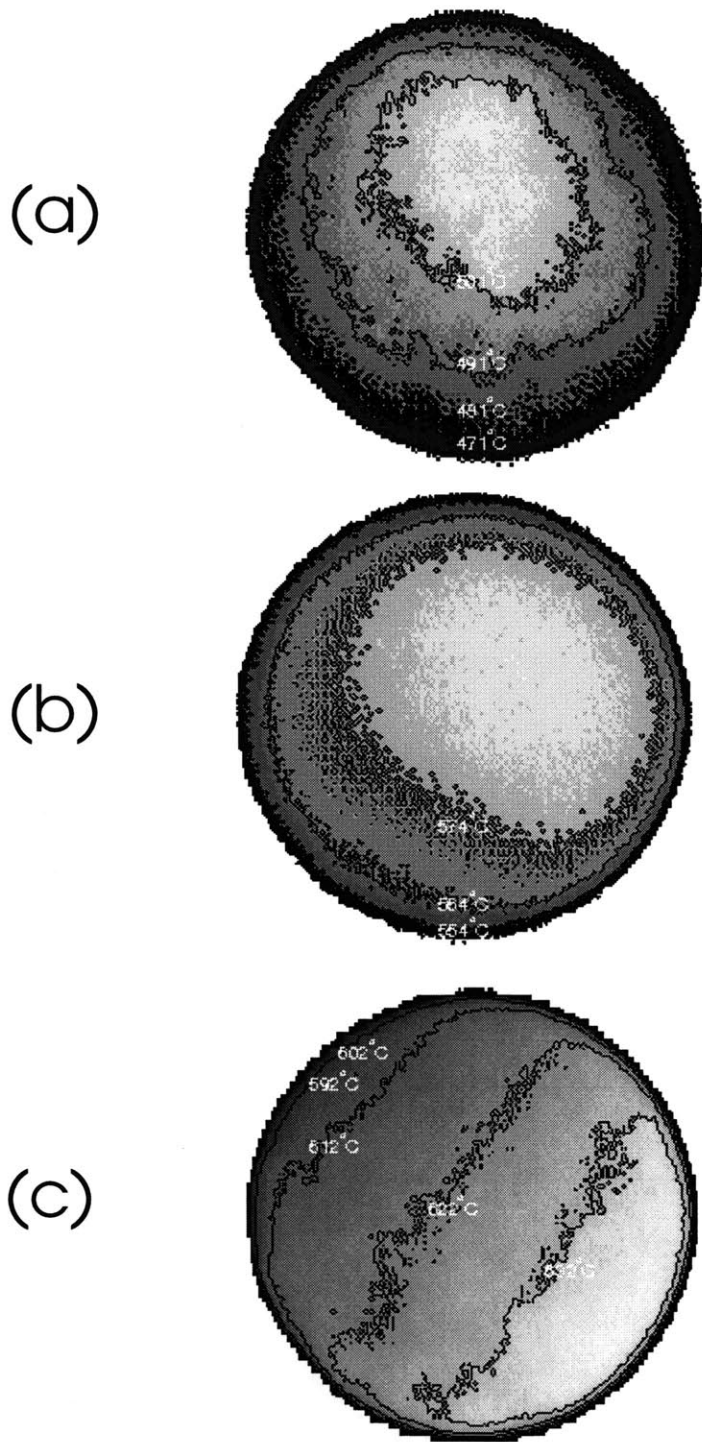


Figure 3-9: Radial Profile of High Temperature Heat Pipe at (a)Top, (b)Midpoint, and (c) Bottom of Cavity

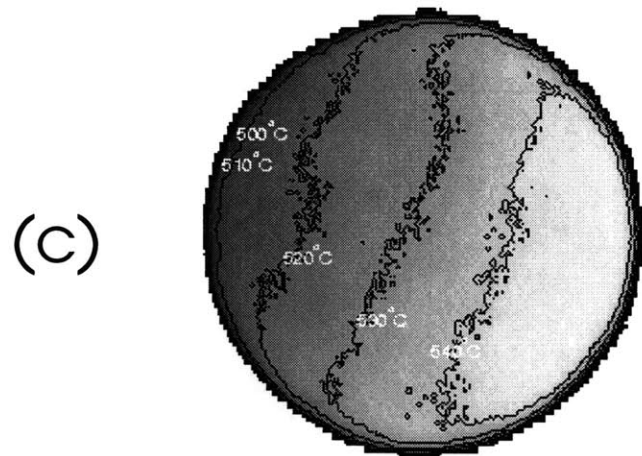
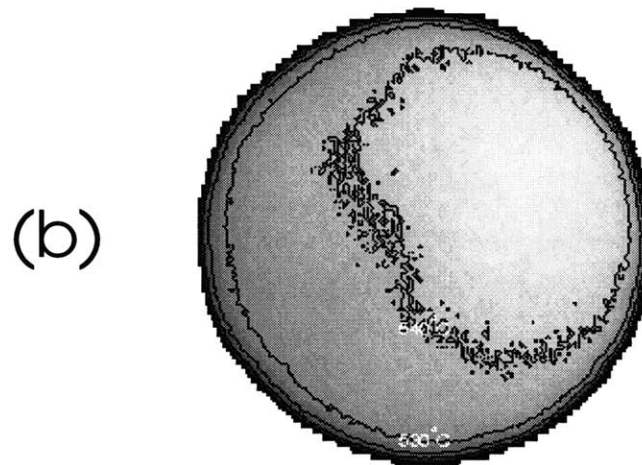
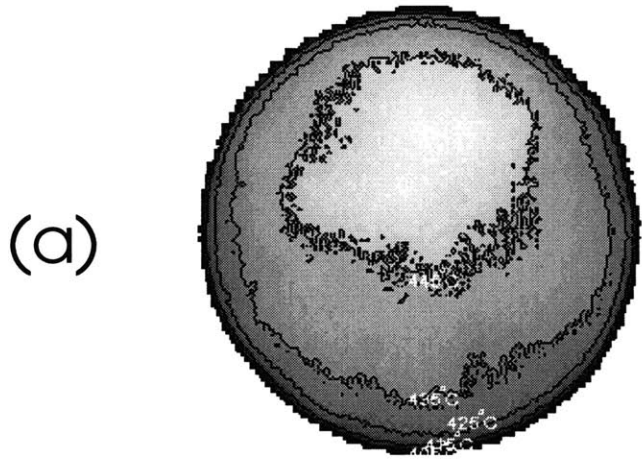


Figure 3-10: Radial Profile of Stainless Steel Cylinder at (a)Top, (b)Midpoint, and (c) Bottom of Cavity

temperature is due to the misalignment of the quartz charge at the bottom of the cavity.

The radial gradient at each axial position is affected by the asymmetry of the thermal profile. The difference between the maximum and minimum temperature varies from 28 to 40 °C. The differences are greater at the ends compared to the axial midpoint. The high temperature heat pipe has a larger temperature difference at the midpoint of the cavity than the stainless steel cylinder.

Chapter 4

Discussion

4.1 Heat Pipe Performance

4.1.1 Outer Surface Measurements

The temperature distributions of the low temperature and high temperature heat pipes were more closely isothermal than those of the stainless steel cylinder. For the low temperature heat pipe at setpoints between 100 °C and 200 °C the axial temperature difference was less than 2 °C. For the high temperature heat pipe at a setpoint of 900 °C the axial temperature difference was less than 5 °C. It is important to note that the heat pipes maintained these small temperature differences with no insulation and with solely the presence of a Au-coated Pyrex radiation shield. It's also notable that these heat pipes did not exhibit the sharp end effects experienced by Bienert [14].

The stainless steel cylinder maintained a linear axial gradient over 60% of it's length above the location of the heater. The magnitude of the gradient, as calculated from Figure 3-8 is 13.5 °C/cm. The magnitude of the gradient is set by the thickness, material, and power input to the cylinder. If the axial gradient is obtainable within the desired range for a crystal growth process it may be advantageous to use a \$60 cylinder rather than a \$2000 heat pipe.

Figures 3-3 through 3-6 show that the circumferential temperature variation is

less than 4 °C at setpoints between 100 °C and 200 °C. Both the low temperature heat pipe and the stainless steel cylinder show this low variation. This suggests that a heat pipe is not necessary to maintain a circumferential isothermality if the heating element is designed symmetrically.

The sharp temperature difference between the inner and outer walls of the heat pipe, shown in Table 3.1, is caused by lack of insulation. There was no way to avoid this without obstructing the optical line of site required for infrared measurement. The fact that the heat pipes were axially isothermal suggests that the vapor space was also isothermal, as would be predicted by Faghri in Figure 1-7.

4.1.2 Interior Radial Profiles

The radial gradient measurements show a smaller radial gradient at the midpoint of the stainless steel cylinder than the high temperature heat pipe. This is due to lower inner wall temperature of the stainless steel cylinder than the high temperature heat pipe, caused by smaller thermal conductivity of the stainless steel. The radial gradient would be smaller at all points in the furnace if the diameter of the quartz charge were nearer to the inner diameter of the furnace cavity which would reduce convective heat losses.

The magnitude of the radial gradient on the quartz charge was greater at the top than at the bottom of the cavity. Only the top surface of the quartz charge was imaged. Heat transport to the imaged surface was composed of radiation and conduction from within the charge material below the surface and radiation and convection from the furnace cavity above the surface. When the imaged surface was located at the bottom of the cavity the heat flow was more uniformly distributed over the surface caused the radial gradient to be minimized.

4.2 Infrared Thermography

Infrared thermography was shown to be capable of collecting real time temperature data on isothermal furnace liners. The camera is most useful in determining relative

temperature information, such as gradients. Absolute temperature measurements require precise knowledge of the spectral and thermal emissivity of the surface. The greybody assumption can be used with an associated loss of precision. A contact thermocouple can be used to calibrate the infrared camera, but the thermocouple must be in close thermal contact with the heat pipe.

The non-symmetry of radial profiles, particular those at the bottom of the cavity in Figures 3-9 (c) and 3-10 (c) is caused by a mis-alignment of the heat pipe assembly with the quartz charge. Infrared thermography is capable of giving a better picture of radial symmetry than can be measured with thermocouples.

The principal disadvantage of infrared thermography is the need to maintain a clear optical path to the observed component. This limits the use of insulation materials. In this work it was shown to be a non-critical issue because of the capability of the heat pipes to approach isothermality without insulation.

A low temperature coating with a measured emissivity of 0.88 was used with the low temperature heat pipe and stainless steel cylinder at setpoints 100 to 200 °C. A ceramic coating was used for high temperature measurements and was used to make relative temperature measurements at a setpoint of 900 °C. Accurate emissivity measurement of surface coatings are needed to provide absolute temperature measurements with infrared thermography.

Chapter 5

Conclusions/Recommendations

The low temperature CuNi/water heat pipe exhibited axial and circumferential temperatures within 2 °C at setpoint temperatures from 100 °C to 200 °C. The high temperature Inconel/Na heat pipe exhibited axial temperatures within 5 °C at setpoint temperature of 900 °C. This is an improvement over the stainless steel cylinder which varied over 20 °C at low temperature and 100 °C at high temperature.

Both the high temperature heat pipe and the stainless steel cylinder caused a quartz charge to experience a radial temperature difference between 28 to 40 °C. The high temperature heat pipe had a smaller gradient at the midpoint of the furnace cavity than the stainless steel cylinder. The high temperature heat pipe and the stainless steel cylinder were radially symmetric within the furnace cavity.

It is recommended that future work should center on improving the capability of the infrared camera. An improved camera would have high spatial resolution with less noise. In particular, an improved method for assessing the thermal emissivity of the charge materials should be developed. The infrared thermography system can be modified to measure radial profiles in two-zone, Bridgman configuration rather than in the one-zone configuration as it is now constructed.

Bibliography

- [1] J. C. Brice. *Crystal Growth Processes*. Halsted Press, New York City, 1986. ISBN 0470202688.
- [2] J.R. Carruthers. Origins of convective temperature oscillations in crystal growth melts. *Journal of Crystal Growth*, 32:19–26, 1976.
- [3] A.S. Jordan, R. Caruso, and A.R. Von Neida. A thermoelastic analysis of dislocation generation in pulled GaAs crystals. *Bell System Technical Journal*, 59(4):593–637, April 1980.
- [4] K.W. Kelly, K. Koai, and Motakef S. Model based control of thermal stresses during LEC growth of GaAs. *Journal of Crystal Growth*, 113:254–274, 1991.
- [5] G.M. Grover, T.P. Cotter, and G.F. Erickson. Structure of very high thermal conductance. *Journal of Applied Physics*, 35(6):1990–1991, 1964.
- [6] R.S. Reid, M.A. Merrigan, and J.T. Sena. Review of liquid metal heat pipe work at Los Alamos. In M.S. El-Genk, editor, *Proc. of the 8th Symposium on Space Nuclear Power and Propulsion*, number 217 in AIP Conference Proceedings, pages 999–1008, Albuquerque, NM, January 1991. American Institute of Physics.
- [7] W.B. Bienert, G.Y. Eastman, D.M. Ernst, R.W. Longsdorff, and E.A. Scicchitano. From concept to consumer - the commercialization of technology. In *Proceedings of the 31st Intersociety Energy Conversion Engineering Conference*, volume 4, pages 2335–2340, New York City, August 1996. IEEE, IEEE.

- [8] P.D. Dunn and D.A. Reay. *Heat Pipes*. Pergamon Press, London, fourth edition, 1994. ISBN 0080419038.
- [9] S.W. Chi. *Heat Pipe Theory and Practice: A Sourcebook*. Series in Thermal and Fluids Engineering. McGraw-Hill, New York City, 1976. ISBN 0070107181.
- [10] A. Faghri and S. Thomas. Performance characteristics of a concentric annular heat pipe: Part I - experimental prediction and analysis of the capillary limit. *Journal of Heat Transfer*, 111(4):844–850, November 1989.
- [11] A. Faghri. Performance characteristics of a concentric annular heat pipe: Part II - vapor flow analysis. *Journal of Heat Transfer*, 111(4):851–857, November 1989.
- [12] A. Faghri. Vapor flow analysis in a double walled concentric heat pipe. *Numerical Heat Transfer*, 10:583–595, 1986.
- [13] A. Faghri and S. Parvani. Numerical analysis of laminar flow in a double-walled annular heat pipe. *Journal of Thermophysics*, 2(3):165–171, April 1988.
- [14] W. W. Bienert. Isothermal heat pipes and pressure controlled furnaces. *Journal of Thermometry*, 2(1):32–52, 1991.
- [15] E.P. Martin, A.F. Witt, and J.R. Carruthers. Application of a heat pipe to czochralski growth: Part I - growth and segregation behavior of Ga-doped Ge. *Journal of the Electrochemical Society*, 126(2):284–287, February 1979.
- [16] J.A. Burton, R.C. Prim, and W.P. Slichter. Segregation coefficients. *Journal of Chemical Physics*, page 1987, 1953.
- [17] N. Yemenidijan and B.A. Lombos. Heat pipe assisted zone melter for GaAs. *Journal of Crystal Growth*, 46(1):163–168, January 1982.
- [18] W.G. Pfann. *Zone Melting*. John Wiley and Sons, New York City, 1958.
- [19] M.J. Wargo and A.F. Witt. Real time thermal imaging for analysis and control of crystal growth by the Czochralski technique. *Journal of Crystal Growth*, 116(2):213–224, Jan 1992.

- [20] Dynatherm Corporation, Cockeysville, MD, 21030-0398.
- [21] U.S. Patent 3,677,329.
- [22] Inframetrics Corporation, 15 Esquire Road, N Billerica, MA 01862.
- [23] Azonix Corporation, 900 Middlesex Turnpike, Bldg 6, Billerica, MA 01821.
- [24] Leeds and Northrup, North Wales, PA 19454.
- [25] Halmar Electronics, 900 North Hague Ave., Columbus, OH 43204.
- [26] Thermcraft, Inc., P.O. Box 12037, 3950 Overdale Road, Winston-Salem, NC, 27117.